AIAA JOURNAL
Vol. 40, No. 11, November 2002

Sensitivity of Turbulence in Transpired Channel to Injection Velocity Small-Scale Nonuniformity

Zhiqun Deng,* Ronald J. Adrian,† and Christopher D. Tomkins*
University of Illinois at Urbana–Champaign, Urbana, Illinois 61801

Turbulence in a channel flow with a fully transpired wall has been investigated experimentally. Two-dimensional particle image velocimetry is used to measure the instantaneous flowfields within the channel for two different porous surfaces: a 6.35-mm honeycomb and a 3.175-mm honeycomb. The 6.35-mm honeycomb creates a larger fluctuation of the injection velocity than the 3.175-mm honeycomb by a factor of 1.7. The boundary conditions on the porous surface are very important to the internal core flow evolution and flow pattern. For a coarse porous surface (the 6.35-mm honeycomb with higher perturbation level on the transpiration surface), the mean flow differs significantly from the classical laminar solution and computational results, and much more turbulent shear stress is indicated. However, with small pore size (the 3.175-mm honeycomb, with relatively lower perturbation level on the surface), the mean velocity profiles are very close to the analytical laminar solution for a considerable downstream length, and the turbulent shear stress is much smaller than in the first case. Therefore, profound modification of the flow structure can occur due to the effect of nonideal wall boundary conditions on the porous surface.

Nomenclature

D	=	pipe diameter
H	=	channel height
I_t	=	rms value, $\sqrt{(\sigma_u^2 + \sigma_v^2)}$
L	=	channel length
P	=	mean pressure
Re_w	=	mean injection Reynolds number for porous pipe, $V_w D/(2\nu)$, channel with two injection walls, $V_w H/(2\nu)$, and channel with one injection wall, $V_w H/\nu$
T	=	temperature of fluid
$U_{\max}$	=	maximum local mean streamwise velocity
U, V	=	mean streamwise and vertical velocity
u', v'	=	turbulent velocity fluctuations about the mean
$\overline{u'v'}$	=	Reynolds shear stress
V_w	=	mean injection velocity on the porous surface
$\underline{x}$	=	(x, y, z)
β	=	momentum flux factor
ν	=	kinematic viscosity of fluid
σ_u	=	rms of u', $\sqrt{\overline{u'^2}}$
σ_v	=	rms of v', $\sqrt{\overline{v'^2}}$

Introduction

FLOW in the core of a solid rocket motor is an unusual form of wall turbulence because the turbulence is created by the release of gas normal to the wall, as opposed to friction associated with flow parallel to the wall. Consequently, conventional turbulence modeling is suspect. This paper describes experiments conducted to provide insight into the essential features of such flows for the purpose of supporting the development and validation of numerical computations based on Reynolds averaged Navier–Stokes (RANS) and large-eddy simulation. This study uses a cold, incompressible flow produced by a single transpired wall in a rectangular cavity (Fig. 1), which has turbulence production similar to the more complicated reacting flow. It is found that the details of the wall boundary condition, in the form of the amplitude and scale of the flow perturbations at the wall, have a profound effect on the turbulent flow in the core. Two different transpiration surfaces are used to investigate this effect. Measurements of the instantaneous velocity field using two-dimensional particle image velocimetry (PIV) indicate flow behavior ranging from negligible turbulence effect with a nearly laminar velocity profile to a strongly turbulent flow with a very blunt mean velocity profile, depending on the surface.

Taylor[1] and Culick[2] deduced the inviscid, laminar, self-similar solution to the problem of core flow within a cylindrical chamber with uniform wall injection. This solution can also be found easily for the case of the rectangular channel. Dunlap et al.[3] investigated how well Culick's[2] solution simulates actual viscous laminar flow in a circular pipe, using sintered bronze (with very fine pore size) as the porous material, and found that the experimental results agreed strikingly well with the prediction. To explain this agreement, the authors[3] noted that the net viscous force acting on a small fluid element is negligible compared with the net pressure force. Several other experiments have been carried out to study the core flow, with different measurement techniques and experimental apparatus. Some details are shown in Table 1. Olson and Eckert[4] investigated the flowfield in a porous pipe and found that the flow pattern without entrance, as in a rocket, was very different from that with entrance flow. Yamada and Goto[5] examined the axial and normal velocity profiles and turbulence intensity profiles in an investigation of erosive burning in a two-dimensional channel with side injection. Dunlap et al.[6] measured the turbulence properties at various downstream locations in a cylindrical chamber with relatively low injection velocity.

Regarding transition, Beddini[7] predicted three regions of behavior: region 1, farthest upstream, in which the laminar theory holds; region 2, called the transition region, in which the mean velocity profiles and turbulent statistics undergo transition from the laminar case; and region 3, after the transition region, in which turbulence dominates, and the velocity profiles become steeper close to the wall. Similar transition behavior was also observed in the experiments at high injection Reynolds numbers performed by Traineau et al.[8] However, the transition points predicted by different authors vary significantly, depending on the facility and simulation.

The aim of this paper is to report a remarkable change in the mean velocity profile and turbulent shear stress profile of the turbulence that is caused by seemingly unimportant changes in the pore size of the transpired wall. Two types of porous surfaces are used: a 6.35-mm honeycomb and a 3.175-mm honeycomb. Both honeycombs have open area of about 72%. These pore sizes are

Received 5 December 2000; presented as Paper 2001-1019 at the AIAA 39th Aerospace Sciences Meeting, Reno, NV, 8–11 January 2001; revision received 21 June 2002; accepted for publication 25 June 2002.

*Ph.D. Student, Department of Theoretical and Applied Mechanics, Center for Simulation of Advanced Rockets.

†Professor, Department of Theoretical and Applied Mechanics, Center for Simulation of Advanced Rockets. Associate Fellow AIAA.

Table 1 Previous experimental investigations of internal flows related to solid rocket motor

Author(s)	Year	Geometry	Range of Re_w	Measurement technique	Quantities measured	Porous surface	Pore size, μm
Olson and Eckert[4]	1966	Pipe $L/D=24$	250–7500	Impact tube	U, V, T, β	Cloth wrapping	N/A
Yagodkin[11]	1967	Pipe $L/D=30$	At least 130	Hot-wire photograph	U, V, σ_u, σ_v	Carbon, metals	N/A
Dunlap et al.[3]	1974	Pipe $L/D=8.4$	300–2500	Hot wire	U, V, σ_u, σ_v	Sintered bronze	5–15
Yamada and Goto[5]	1976	Two-dimensional channel $L/H=10$	N/A	Hot wire	$U, V, \sigma_u, \sigma_v, I_t$	N/A	20 70
Traineau et al.[8]	1986	Two-dimensional channel $L/H=24$	7840	Two-dimensional laser Doppler velocimetry	$U, V, \sigma_u, \sigma_v, u'v', \beta, I_t$	Sintered copper balls	50
Dunlap et al.[6]	1990	Pipe $L/D=9.5, 14.3$	4500–9000	Three-dimensional hot wire	$U, V, \sigma_u, \sigma_v, \sigma_w, u'v', u'w',$	Sintered bronze	5–15
Cheng and Hwang[9]	1995	Two-dimensional channel $L/H=40$	5–20	N/A	$U, V, T_w, P, T_{\text{exit}}$	Ceramic fiber, graphite plate	N/A
Couton et al.[10]	1996	Two-dimensional channel complex geometery	4900	Two-dimensional laser Doppler velocimetry	$U, V, \sigma_u, \sigma_v, I_t$	Sintered poral, metallic weave	75

Table 2 Dimension data of the honeycombs

Case	Surface	Cell size, mm	Cell pattern	Thickness A, mm	Center spacing, mm	Open area, %
1	6.35-mm honeycomb	6.35	Staggered	152.4	7.144	71.7
2	3.175-mm honeycomb	3.175	Staggered	152.4	3.572	71.7

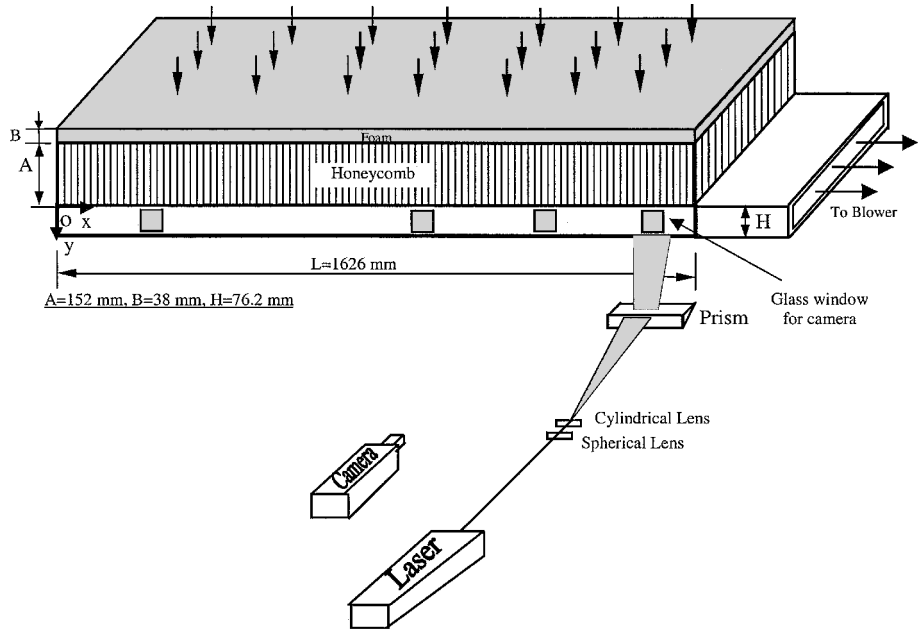

Fig. 1 Schematic of experimental apparatus.

larger than those used in the previous experiments listed in Table 1 (Refs. 3–6 and 8–11) (porous walls with pore size ranging from 5 to 75 μm).

Experimental Appratus and Techniques

Test Channel

The apparatus is shown schematically in Fig. 1. The total length of the channel L is 1626 mm, and the channel height H is 76.2 mm, giving a length to height ratio (L/H) of 21. With a 533-mm width and an aspect ratio of 7, two-dimensional flow is assumed. Air is sucked into the channel through the top foam and the honeycomb by a high-pressure direct-drive blower. The top foam sheet (38 mm in thickness) creates a pressure drop that is large in comparison to the pressure drop due to velocity increase in the channel. Consequently, the injection along the wall is nearly uniform.

Porous Surfaces and Flow Parameters

Two types of porous surface are used: a 6.35-mm honeycomb and a 3.175-mm honeycomb, defined as cases 1 and 2. Both honeycombs are Plascore polycarbonate honeycomb, which has uniform properties and inherently stable cells. Some dimension data and hydrodynamic impedance data are listed in Tables 2 and 3, and important flow parameters are presented in Table 4. Mean values of the wall normal injection velocity V_w in Table 4 are found from two-dimensional control volume analysis by integrating through streamwise mean velocity profiles at four downstream locations. The value of V_w found at the four different locations is constant to within $\pm 5\%$ peak to peak.

Measurement Techniques

With two-dimensional digital PIV, the instantaneous flowfields are measured in the streamwise-normal (x–y) plane at four different downstream locations with injection Reynolds numbers $V_w H/\nu = 1531$ for case 1 and 1566 for case 2. Optical access is obtained through a single glass window inserted into the bottom of the channel and four glass windows in the side wall. The TSI PIV system used in this paper has an acquisition rate of 15 Hz. Approximately 1000 instantaneous fields are used to calculate the mean velocity profiles and statistics for each location. Prasad et al.[12] showed that the random error associated with particle displacement

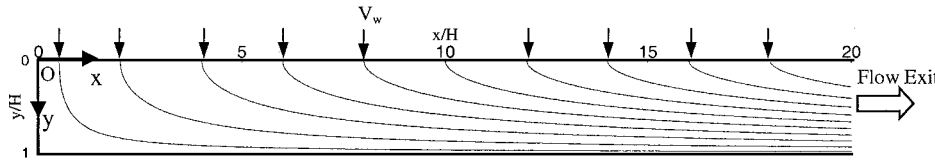

Fig. 2 Streamlines of analytical solution to inviscid, zero Reynolds stress channel flow with steady, uniform one-sided injection.

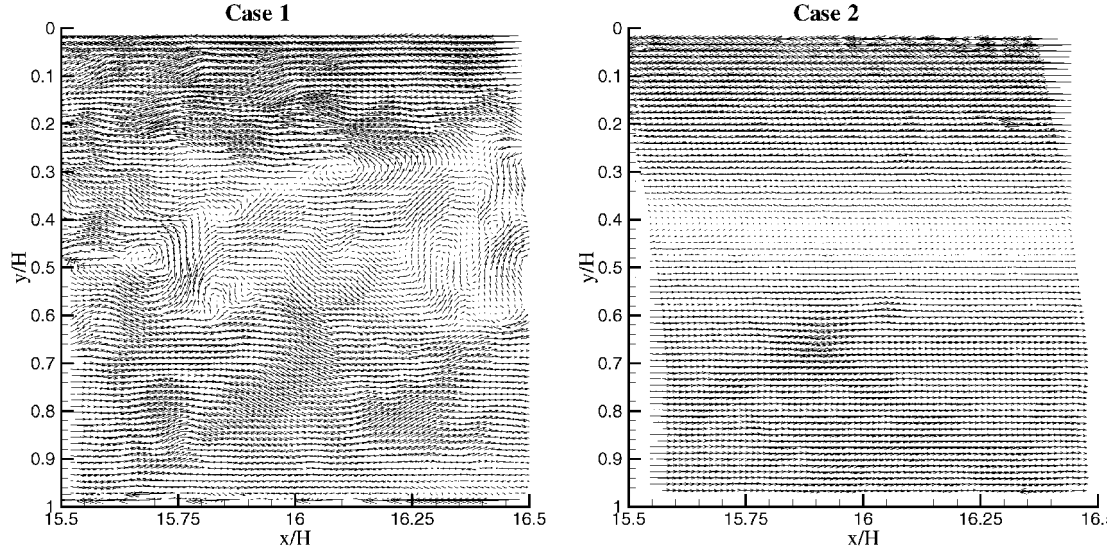

Fig. 3 Instantaneous velocity vector maps for the two test cases.

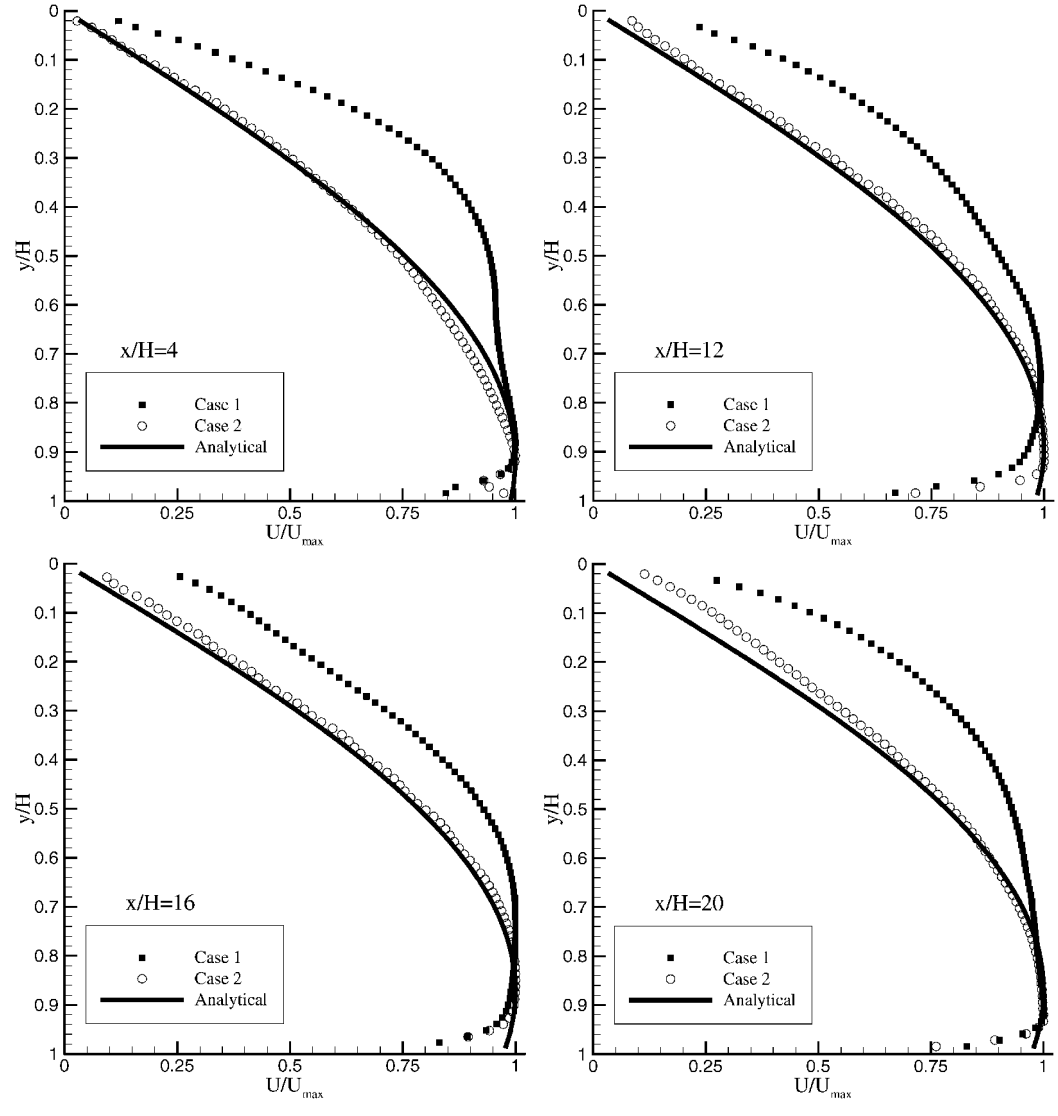

Fig. 4 Mean velocity profiles at different downstream locations.

Table 3 Hydrodynamic impedance of the honeycombs

Impedance	Zero-frequency hydrodynamic impedance dP_w/dV_w, Pa/(m/s)
Case 1	
Surface, 6.35-mm honeycomb	27
Foam	1929
Total	1956
Case 2	
Surface, 3.175-mm honeycomb	124
Foam	1942
Total	1966

Table 4 Experimental flow parameters

Case	Re_w V_wH/ν	Injection velocity V_w, m/s	U_{max}, m/s $x/H=4$	$x/H=12$	$x/H=16$	$x/H=20$
1	1531	0.307	1.31	4.02	5.16	6.80
2	1566	0.312	1.52	4.38	5.96	8.04

estimation in PIV using simple cross correlation is approximately 5% of the particle image diameter. In this study, the particle images are roughly 2 pixels in diameter, so that the rms random error is about 0.1 pixels. Furthermore, because the maximum particle displacements in the PIV measurements are 10 pixels, the relative uncertainty in the PIV measurement of single instantaneous velocity vector due to error in measuring displacement is approximately 1% of the full-scale velocity. These random errors average to zero. There are also bias errors in PIV that do not average to zero. These are estimated to be less than 1% of full-scale velocity.[13]

Results and Discussion

Laminar Solution

A solution can be obtained by applying Culick's analysis[2] to the rectangular channel with one transpired wall as shown in Fig 2. The solution is equivalent to solving the inviscid mean flow, RANS equations with zero Reynolds stress. The mean velocities are given by

$$U(x, y) = (V_w \pi x/2H) \sin(\pi y/2H) \tag{1a}$$

$$V(x, y) = V_w \cos(\pi y/2H) \tag{1b}$$

The streamlines as predicted by the preceding equations are plotted in Fig. 2.

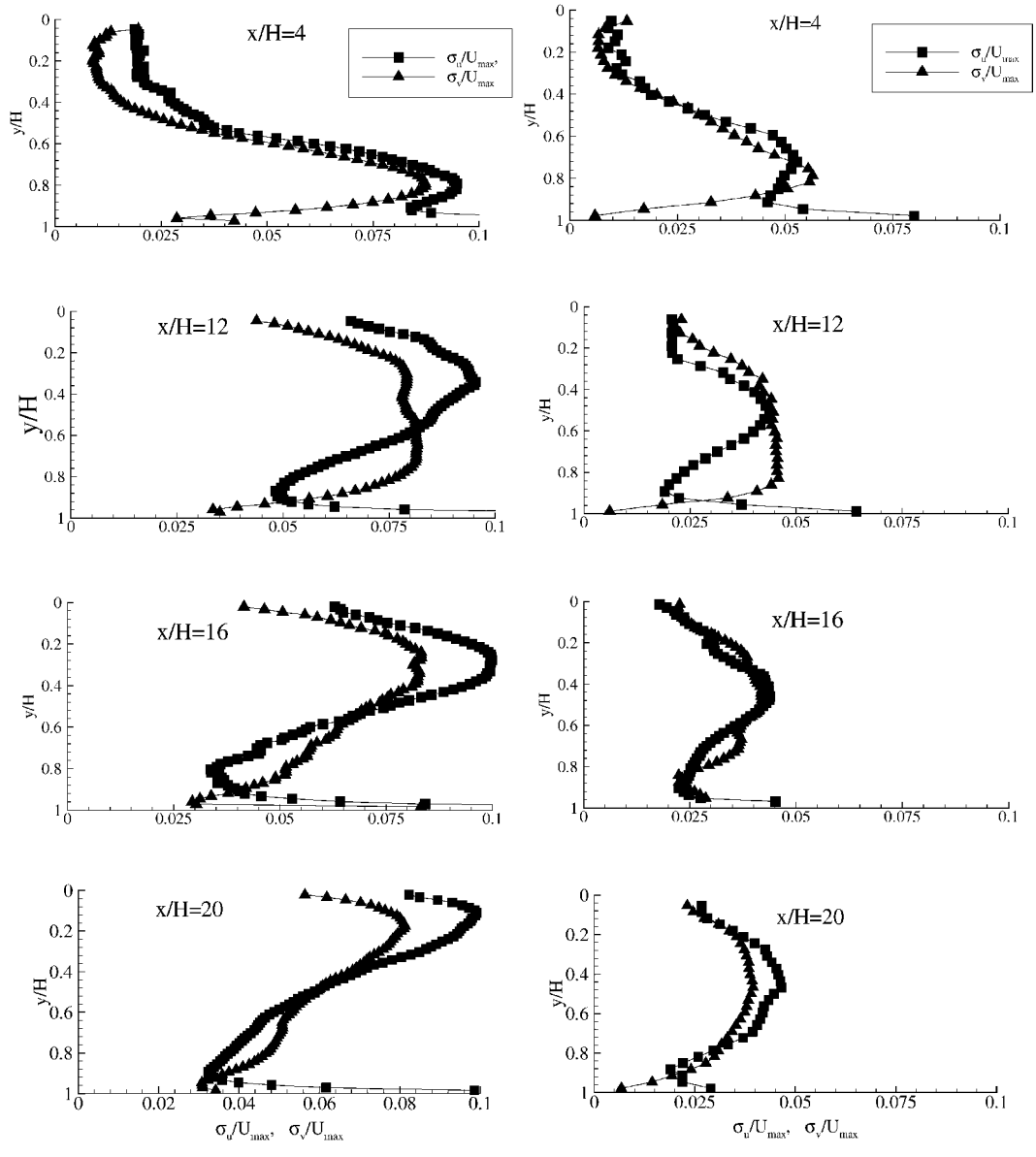

RMS velocity profiles for case 1 at $Re_w = 1531$ RMS velocity profiles for case 2 at $Re_w = 1566$

Fig. 5 RMS velocity profiles at different downstream locations.

Instantaneous Velocity Fields

Two typical instantaneous velocity vector maps captured for the two different porous surfaces are shown in Fig. 3. A constant velocity (area average)[14] is subtracted from the original vector field to better reveal the differences of the two cases. For the case of a 6.35-mm honeycomb (case 1), a very large turbulence level is observed. However, if the interface is replaced by a 3.175-mm honeycomb (case 2) the instantaneous velocity fields change drastically, as shown in Fig. 3, and the flow pattern becomes much smoother and closer to laminar flow. Therefore, the level of turbulence varies significantly with the two different injection boundary conditions.

Mean Flow Properties

Figure 4 shows profiles of the mean streamwise velocity normalized by local maximum streamwise velocity at four different locations. For comparison, the analytical inviscid Reynolds stress-free solution is included, and the effect of the bottom boundary layer is excluded, by taking out the bottom boundary-layer thickness from the channel height H. All of the profiles are normalized by local maximum streamwise mean velocity. The profile of the flow created using the 3.175-mm honeycomb as the porous surface (case 2) agrees well with inviscid Reynolds stress-free solution. The flatter, more turbulent profile corresponds to the 6.35-mm honeycomb (case 1). It can be concluded that with case 2 (less perturbation on the injection boundary), the mean velocity profiles agree well with the inviscid stress-free solution for a considerable downstream distance. However, if the porous surface is very coarse, and more fluctuations are created on the injection surface (case 1), the mean velocity profiles deviate significantly from the analytical stress-free solution and look much more like the flat profiles of fully turbulent channel flow. Clearly, the details of the transpired wall boundary conditions are very important, and nonideal wall boundary conditions can result in substantial modification in the flow structure.

Turbulence Properties

Figures 5 and 6 describe, respectively, profiles of the rms velocity and the Reynolds shear stress at $x/H = 4$, 12, 16, and 20. It is apparent that there is a peak in each profile. Also, when increasing distance increases downstream, the peak moves closer to the transpired surface, consistent with Beddini's computation.[7] More important, case 1 produces significantly higher rms velocities and turbulence shear stresses than case 2.

Figure 7 is obtained by averaging $\overline{v'^2}$ $(x, y/H = 0.08)$ at different downstream locations for both cases and using the maximum value of $\overline{u'v'}$ $(x/H = 20)$ to relate the perturbation near the injection surface to turbulent shear stress thereafter. Both quantities are normalized by the square of the mean injection velocity V_w^2. It is obvious that case 2, with the higher perturbation level near the transpiration surface, causes higher turbulent shear stress than case 1, with a relatively lower perturbation.

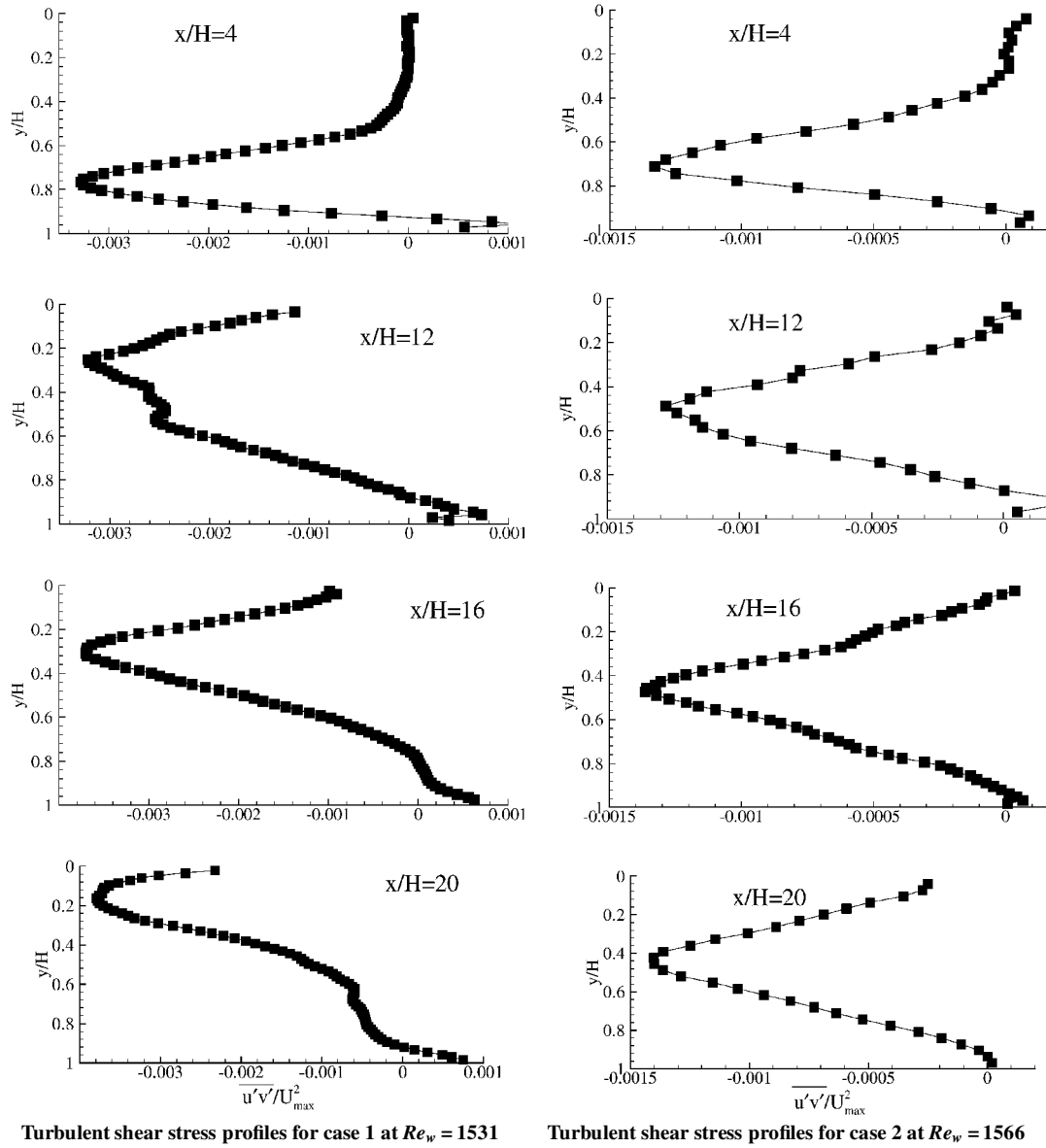

Turbulent shear stress profiles for case 1 at $Re_w = 1531$ **Turbulent shear stress profiles for case 2 at $Re_w = 1566$**

Fig. 6 Turbulent shear stress profiles at different downstream locations.

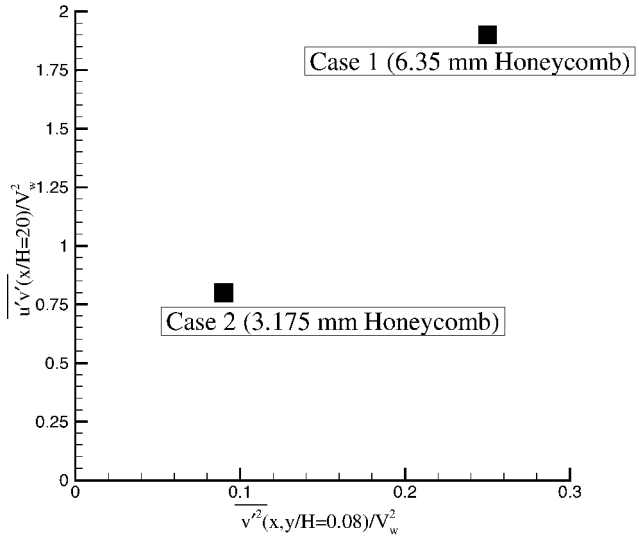

Fig. 7 Relation of turbulent shear stress and perturbation near the porous surface.

Summary

Turbulence in a channel flow with a fully transpired wall depends strongly on details of the transpired wall boundary conditions. With small pore size and small perturbation on the injection surface, mean velocity profiles agree well with the analytical solution for an inviscid Reynolds stress-free flow for a considerable downstream length. This is because the turbulent Reynolds shear stress is small relative to the mean acceleration and pressure gradient. However, if the porous surface is coarse and, consequently, has higher injection fluctuations, the mean flow differs from the stress-free solution, and much more turbulent shear stress is indicated. In summary, nonideal wall boundary conditions can lead to substantial modification of the flow.

Acknowledgment

This research was supported by the Center for Simulation of Advanced Rockets at the University of Illinois at Urbana–Champaign through a grant from the Accelerated Strategic Computing Initiative Program of the U.S. Department of Energy.

References

[1]Taylor, G. I., "Fluid Flow Regions Bounded by Porous Surfaces," *Proceedings of the Royal Society of London*, Series 234A, Vol. 11199, 1956, pp. 456–475.

[2]Culick, F. E. C., "Rotational Axisymmetric Mean Flow and Damping of Acoustic Waves in a Solid Propellant Rocket," *AIAA Journal*, Vol. 4, No. 8, 1966, pp. 1462–1464.

[3]Dunlap, R., Willoughby, P. G., and Hermsen, R. W., "Flowfield in the Combustion Chamber of a Solid Propellant Rocket Motor," *AIAA Journal*, Vol. 12, No. 10, 1974, pp. 1440–1442.

[4]Olson, R. M., and Eckert, E. R. G., "Experimental Studies of Turbulent Flow in a Porous Circular Tube with Uniform Fluid Injection through the Tube Wall," *Journal of Applied Mechanics*, Vol. 33, No. 4, 1966, pp. 7–17.

[5]Yamada, K., and Goto, M., "Simulative Study on the Erosive Burning of Solid Rocket Motors," *AIAA Journal*, Vol. 14, No. 9, 1976, pp. 1170–1176.

[6]Dunlap, R., Blackner, A. M., Waugh, R. C., Brown, R. S., and Willoughby, P. G., "Internal Flow Field Studies in a Simulated Cylindrical Port Rocket Chamber," *Journal of Propulsion*, Vol. 6, No. 6, 1990, pp. 690–704.

[7]Beddini, R. A., "Injection-Induced Flows in Porous-Walled Ducts," *AIAA Journal*, Vol. 24, No. 11, 1985, pp. 1766–1773.

[8]Traineau, J. C., Hervat, P., and Kuentzmann, P., "Cold-Flow Simulation of a Two-Dimensional Nozzleless Solid-Rocket Motor," AIAA Paper 86-1447, June 1986.

[9]Cheng, Y. C., and Hwang, G. J., "Experimental Studies of Laminar Flow and Heat Transfer in a One-Porous Wall Square Duct with Wall Injection," *International Journal of Heat and Mass Transfer*, Vol. 38, No. 18, 1995, pp. 3475–3484.

[10]Couton, D., Plourde, F., and Doan-Kim, S., "Cold Gas Simulation of a Solid Propellant Rocket Motor," *AIAA Journal*, Vol. 34, No. 12, 1996, pp. 2514–2522.

[11]Yagodkin, V. I., "Use of Channels with Porous Walls for Studying Flows Which Occur During Combustion of Solid Propellants," *Proceedings of the 18th Astronautics Congress*, Vol. 3, 1967, pp. 67–79.

[12]Prasad, A. K., Adrian, R. J., Landreth, C. C., and Offutt, P. W., "Effect of Resolution on the Speed and Accuracy of Particle Image Velocimetry Interrogation," *Experiments in Fluids*, Vol. 13, No. 2, 1992, pp. 105–116.

[13]Liu, Z. C., Landreth, C. C., Adrian, R. J., and Hanrantty, T. J., "High-Resolution Measurement of Turbulent Structure in a Channel with Particle Image Velocimetry," *Experiments in Fluids*, Vol. 10, No. 6, 1991, pp. 301–312.

[14]Adrian, R. J., Christensen, K. T., and Liu, Z.-C., "Analysis and Interpretation of Instantaneous Turbulent Velocity Fields," *Experiments in Fluids*, Vol. 29, No. 3, 2000, pp. 275–290.

J. P. Gore
Associate Editor